frontiers | Frontiers in Earth Science

TYPE Original Research
PUBLISHED 22 November 2024
DOI 10.3389/feart.2024.1433182

OPEN ACCESS

EDITED BY
Irene Cornacchia,
National Research Council (CNR), Italy

REVIEWED BY
Douaa Fathy,
Minia University, Egypt
Francisco Sanchez Beristain,
UNAM Juriquilla, Mexico

*CORRESPONDENCE
Zhenkui Jin,
296545727@qq.com

RECEIVED 15 May 2024
ACCEPTED 05 November 2024
PUBLISHED 22 November 2024

CITATION
Cheng H, Jin Z, Zhu R, Wang J, Zhu X, Li B and Blaise Ketchaya Y (2024) Depositional model of a bioherm based on factor analysis: a case study in Western Beijing, China.
Front. Earth Sci. 12:1433182.
doi: 10.3389/feart.2024.1433182

Depositional model of a bioherm based on factor analysis: a case study in Western Beijing, China

Hao Cheng[1,2], Zhenkui Jin[1]*, Rukai Zhu[2], Jinyi Wang[1], Xiaoer Zhu[3], Baiqiang Li[4] and Yanick Blaise Ketchaya[4]

[1]College of Geosciences, China University of Petroleum, Beijing, China, [2]China National Petroleum Corporation, Research Institute of Petroleum Exploration and Development, Beijing, China, [3]CNOOC Research Institute Co. Ltd., Beijing, China, [4]School of Earth and Environment, Anhui University of Science and Technology, Huainan, China

As an important type of microbial carbonate, the study of bioherm sedimentary models is of great significance to the exploration and development of carbonate rock. Bioherms from the Lower Zhangxia Formation of the Middle Cambrian Miaolingian were discovered in the Xiaweidian section of Western Hills, Beijing. The stratigraphic sequence from bottom to top consists of micritic oolitic limestones, flat-pebble conglomerates, laminated limestones (bioherm), shales, sparry oolitic limestones, and mud-ribboned limestones. This study uses a range of techniques to analyze the geochemistry of these rocks, including scanning electron microscopy (SEM), X-ray diffraction (XRD), carbon and oxygen isotope analysis, and major and trace element analysis. To ensure the accuracy of the results, factor analysis was used to screen the data and identify the elements that best represent the characteristics of the samples, obtaining the most reliable factors for analyzing the deposition environment and determining the deposition model. Through factor analysis, carbon and oxygen isotopes, Fe, Ti, Ni, and V were selected to reconstruct the paleoenvironment and deposition model. The results suggest that the Zhangxia Formation bioherm formed in the shallow-water environment of the open platform facies at the edge of the carbonate platform, which provides ideal conditions for the growth of microorganisms and the development of extensive bioherms during this time period. Subsequently, as water depth decreased and hydrodynamic and oxidative conditions intensified, the environment became unsuitable for microbial growth, leading to the cessation of bioherm development. This study confirms the effectiveness of numerical analysis methods in reconstructing bioherm deposition model and expands the application of these methods in carbonate studies.

KEYWORDS

factor analysis, depositional model, bioherm, Cambrian, Zhangxia Formation, Beijing

1 Introduction

The Cambrian Sea is known as the "skeleton-poor sea" (Pruss et al., 2010) and stormy sea" (Pratt, 2002; Myrow et al., 2004; Pratt and Bordonar, 2007). The first action of early Phanerozoic cyanobacteria calcification occurred in the early Cambrian (Riding, 2000), which is called the "Cambrian-Early Ordovician Recovery of microbial carbonates (Riding and Liang, 2005; Riding, 2006)." Bioherms studied in this paper are widely developed in

the strata of this period, which are mound-like carbonate geological bodies formed by microorganisms (Riding, 2002; Mei et al., 2023).

Previous studies on bioherms have focused on building microorganisms (Riding, 1991; Leggitt and Cushman, 2001; Katrin et al., 2018; Du et al., 2024; etc.), growth morphology (James and Kobluk, 1978; Woo and Chough, 2010; Aksu et al., 2018; etc.), internal structure (Bourillot et al., 2009; Liu et al., 2024; Yun et al., 2024; etc.), diagenesis (James and Klappa, 1983; Kopaska-Merkel and Haywick, 2001; Bosak et al., 2013; Mei et al., 2023; etc.), and depositional environments (Samankassou, 2001; Gómez-Pérez, 2003; Murphy and Sumner, 2010; Bhat et al., 2012; Wu et al., 2017; Du et al., 2024; Liu et al., 2024; etc.).

Geochemical analysis is often used to analyze depositional environments. Many geochemical characteristics corresponding to depositional environments have been established in previous studies (Octavian and Duncan, 2020). For example, sereval methods which focus on different chemical elements have been proposed to determine redox properties in depositional environments, including V (Wanty and Goldhaber, 1992; Calvert and Pedersen, 1993; Tribovillard et al., 2006), Re (Colodner et al., 1993; Crusius et al., 1996; Yamashita et al., 2007), Cr (Calvert and Pedersen, 1993; Algeo and Maynard, 2004; Tribovillard et al., 2006), U (Myers and Wignall, 1987; Wignall and Twitchett, 1996; McManus et al., 2005; Tribovillard et al., 2006), Mo (Erickson and Helz, 2000), Ni (Huerta-Diaz and Morse, 1992; Calvert and Pedersen, 1993; Tribovillard et al., 2006) and Th/U (Wignall and Twitchett, 1996). However, the content of elements in rocks is affected by many factors; therefore, different elements often show different correlations with the depositional environment. Some geochemical methods may correctly reflect depositional environments, whereas others may not. Therefore, different geochemical methods often produce inconsistent or even contradictory conclusions, and it is difficult to determine which method reflects the truth.

In this study, a factor analysis method is proposed to determine which geochemical elements are reliable for depositional environment analysis. As a case study, this method was applied to analyze the depositional environment of bioherm in the Zhangxia Formation of Cambrian Miaolingian in Western Beijing, China.

2 Geologic background

The study area is located in Xiaweidian Village, about 20 km southwest of Beijing, and belongs to the northern part of North China Platform (Figure 1), with an area of about 1,097,661 km^2 (Chough et al., 2010; Lee et al., 2012). In the Paleozoic, the North China Platform was located in a low-latitude region near the equator and had long been in a zonal environment (Huang et al., 2008). During Series 2 and Miaolingian, the North China Platform was a shallow carbonate platform and suffered further transgressions during the Furongian period (Mei et al., 1997; Chough et al., 2010; Lee et al., 2012). At the end of the Furongian period, the North China platform experienced a sea retreat towards the end of the Cambrian (Figure 2). The Miaolingian includes the Maozhuang Formation (Є3m), Xuzhuang Formation (Є3x), the Zhangxia Formation (Є3z), and Gushan Formation (Є3g). Zhangxia Formation located in the middle-upper part of Miaolingian. The contact among the above formations is conformable.

The Zhangxia Formation is about 120 m thick and consists of thinbedded limestones, flat-pebble conglomerates, and oolites, with dolomitization occurring on some rock surfaces but no obvious diagenetic alteration in the interior of the rock. The bioherms studied in this study occurred in the lower part of the formation (Figure 2).

3 Materials and methods

Sixteen rock samples were collected from the study area for X-ray diffraction (XRD), scanning electron microscopy (SEM), energy dispersive spectrometry (EDS), major and trace element analysis, and carbon-oxygen isotope analysis. All laboratory analyses were conducted at the State Key Laboratory of Petroleum Resources and Prospecting, China University of Petroleum, Beijing, China. To ensure the validity of the data, fresh rock samples were selected to avoid late-stage veins, pore-filling structures, and recrystallized portions. During sample preparation, impurities, such as gravel and dolomite, were removed as much as possible. The rocks were then powdered for the subsequent experiments. Quality control measures for geochemical analysis: All experiments were monitored by randomly inserting parallel samples, and any anomalous data obtained were subjected to multiple repeat experiments to ensure data validity.

3.1 X-ray diffraction (XRD) analysis

The calcite and dolomite contents of the 16 samples were analyzed using X-ray diffraction (XRD). XRD analysis was performed with a BRUKER D2 PHASER diffractometer with CuKα rays of 40 kV and 100 mA to determine the mineralogical composition of the samples. The copper tube was operated at 40-kV and 25-mA beam currents and run at a 2θ angle ranging from 0° to 65° at a rate of 0.8° min^{-1}. Jade 6.0 software was used to perform spectral analysis.

3.2 Stable isotope analysis

A MAT-253 stable isotope mass spectrometer was used for the stable isotope analysis ($\delta^{13}C$ and $\delta^{18}O$). Approximately 4 mg of powdered pure calcite samples was reacted with phosphoric acid at 25°C to produce CO_2, following the method proposed by McCrea (2004). Vienna Pee Dee Belemnite (V-PDB) was used as the standard for C isotopes, and V-PDB and Vienna Standard Mean Ocean Water (V-SMOW) were used as the standards for O isotopes. All values were recorded per mill (‰) relative to the Pee Dee Belemnite (PDB) standard. The analytical precision for both $\delta^{13}C$ and $\delta^{18}O$ values was greater than ± 0.1‰.

3.3 Major and trace elements analysis

The major and trace elements (Ca, Mg, Mn, K, Na, Si, Fe, Sr, Ba, etc.) were measured using an inductively coupled plasma optical emission spectrometer (ICP-OES) (Thermo Fisher IRIS Advantage) and inductively coupled plasma mass spectrometry

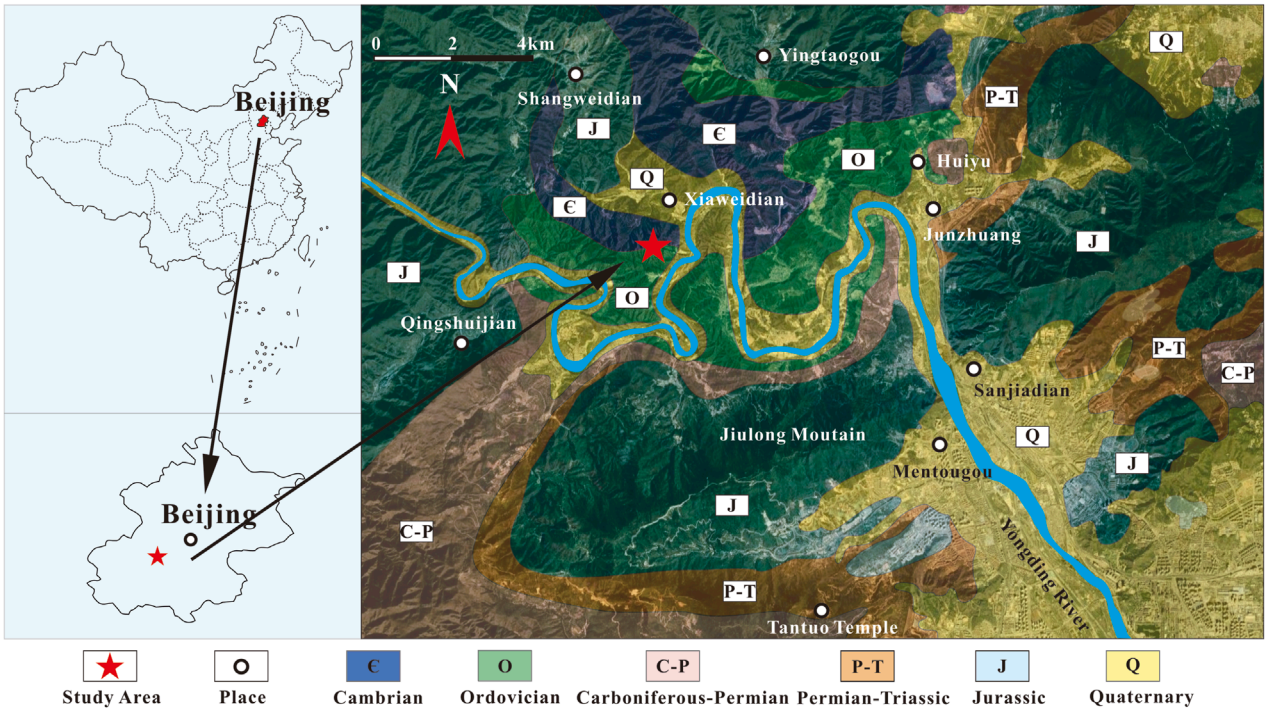

FIGURE 1
Location of study area and distribution of strata.

(ICP-MS) (Thermo Fisher VG-X7). Samples were pretreated with HF+HNO_3 mixed acid prior to analysis. International standards (GSR-5, GSR-6, and GSD-9) and blank samples were used for monitoring. The relative standard deviations of the major and trace element analyses were less than 1% and 2%, respectively.

3.4 Factor analysis

This study uses a factor analysis method to determine which elements and geochemical methods are reliable for analyzing depositional environment.

Factor analysis, or R-Q factor analysis, is a data simplification technique that extracts common factors from various groups. It explores the basic structure of observed data by studying the internal dependence relationship between variables, and uses a few factors to reflect the primary information of many original variables (Filzmoser et al., 2009; Alhija, 2010). Factor analysis has the following advantages: (1) the number of factors is much smaller than that of the original variables; (2) factors are not a simple choice of original variables, but a new synthesis; (3) there is no linear relationship between the factors; and (4) factors can be interpreted clearly, maximizing the role of professional analysis (Alhija, 2010).

Principal factor analysis includes R-type factor analysis of variable correlation and Q-type factor analysis of sample correlation. The analysis variables were selected to calculate the R-type and Q-type factor loading matrices. Subsequently, a planar graph was drawn with Q-type factor loads F0 and F1 of the sample, and the correlation coefficient matrix of the original variables was calculated. After selecting the analysis variables, R-type factor loads were projected onto the graph. After factor rotation, a scatter chart of the variables and samples was generated, and the factor score was calculated (Filzmoser et al., 2009). Accordingly, correlation statistics and analyses between variables and samples were carried out, and then the objective classification results of the samples were explored (Grunsky, 2010; State, 2015; Wang et al., 2017). The detailed calculation procedure for factor analysis is shown in the Supplementary Appendix.

4 Results

4.1 Microscopic image

Abundant bioherms developed in a layer about 2.0 m thick in the lower Zhangxia Formation. Each bioherm is about 1.5 m~1.7 m high and 3.0 m~5.0 m wide (Figure 3). Most bioherms were surrounded by green shales. The distance between bioherms was usually several meters (Figure 3A). Bioherms consisted of concentric layers (Figure 3B), but the concentric structure of some bioherms was not very obvious. The rock formed by the bioherm is laminated limestone. Dolomitization occurs on the limestone surface to form brown mottling (Figure 3C). The diameter of the mottles is usually about 1 cm. Laminated limestone is homogeneous, dense, and nonporous. Under the microscope, light colored mottles are composed of cryptocrystalline calcite and dark colored mottles are composed of microcrystalline calcite (Figure 4A). Dark colored mottles contain trilobite fossils, while light colored mottles contain

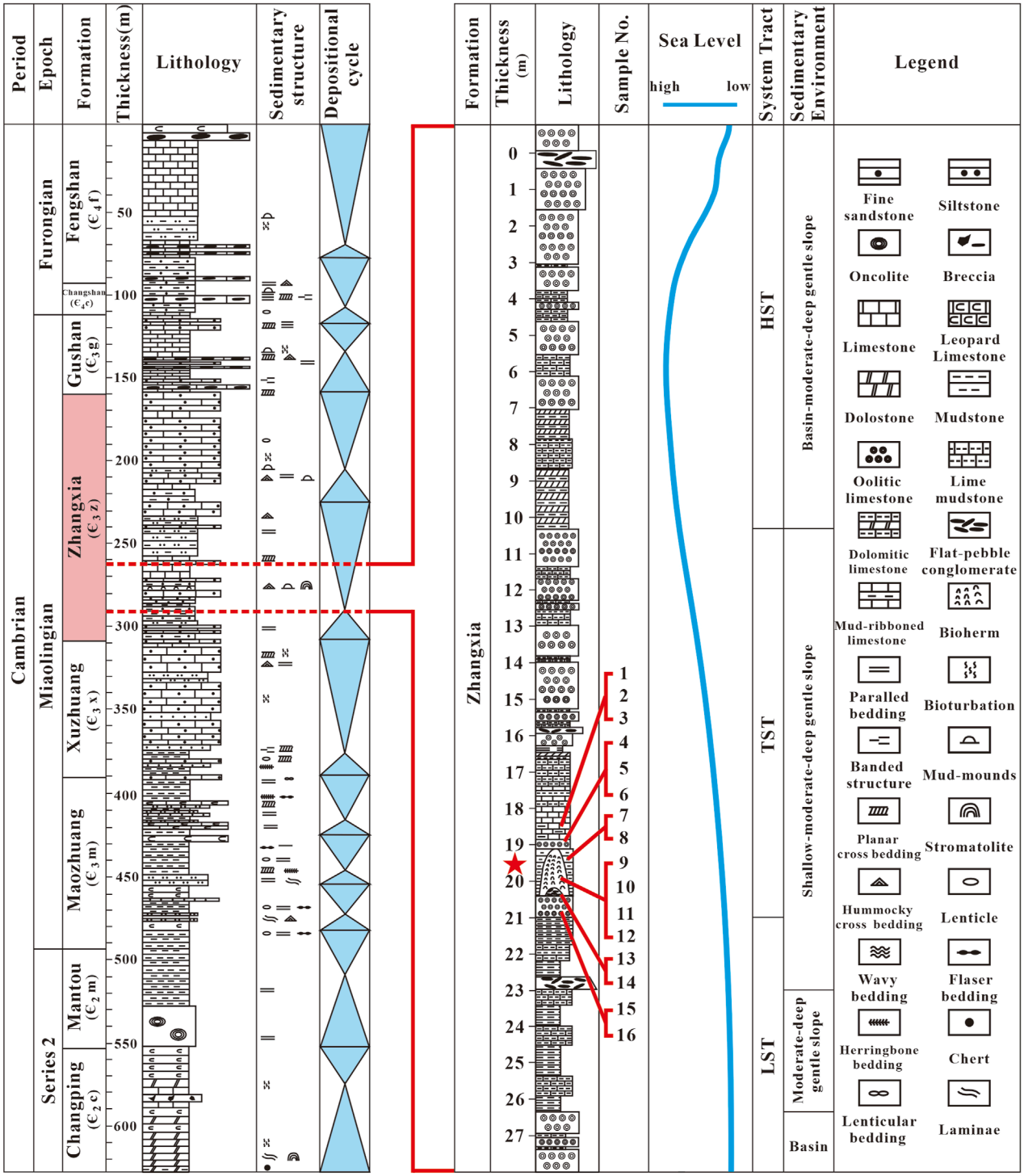

FIGURE 2
Cambrian stratigraphy of study area and detailed stratigraphic section of Zhangxia Formation.

no fossils. Some samples contained trace amounts of pyrite in light colored mottles.

The substrates of the bioherms were flat-pebble conglomerates and micritic oolitic limestones (Figure 3). In flat-pebble conglomerate, clusters are typically 0.4 cm × 3.0 cm–0.8 cm × 5.0 cm in size and randomly oriented. The matrix of flat-pebble conglomerates is micritic calcite. Ooids in sparry oolitic limestone are 0.2 mm–0.5 mm in diameter, and the matrix among the ooids is micritic calcite (Figure 4B).

The surrounding rock of the bioherm is dark green shale, and the overlying strata of the shale are sparry oolitic limestone and mud-ribboned limestone (Figure 3). Lamination

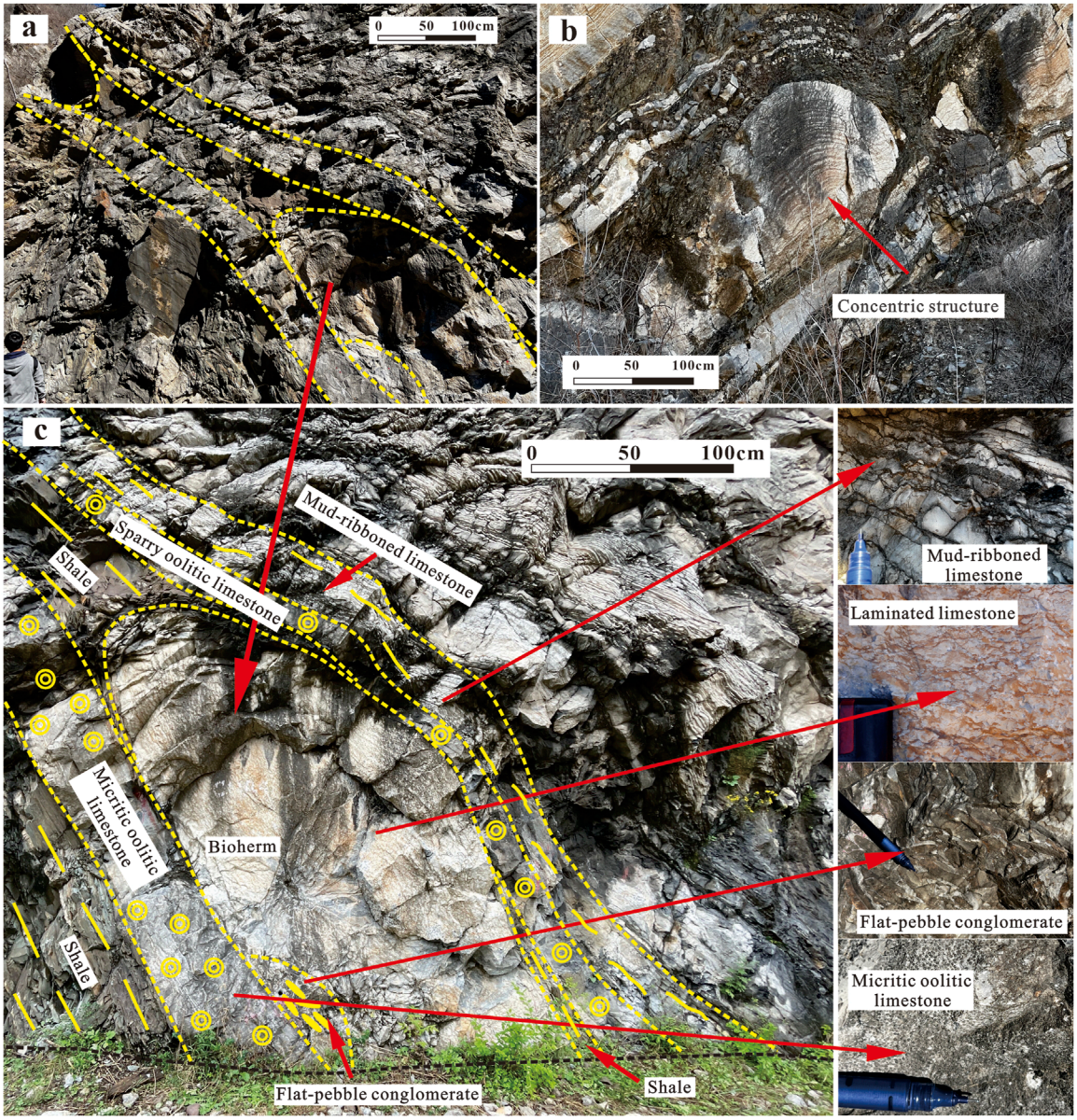

FIGURE 3
Characteristics of bioherms in Xiaweidian, Western Hill, Beijing, China. **(A)** Distribution characteristics of bioherms; **(B)** Concentric structure of bioherms; **(C)** The overlap of strata in the study area.

in the shale was not apparent. The shales pinch out towards the bioherms at the bottom and top (Figure 3). Some ooids in sparry oolitic limestone were selectively dolomitized (Figure 4C). The mud-ribboned limestone is mainly composed of recrystallized microcrystalline calcite, and the mudzone is mainly composed of clay (Figure 4D).

4.2 Geochemical data

XRD analysis of the 16 samples indicates that the main components of the 14 limestone samples are calcite with a high content (76.1%–89.2%, 84.80% on average), and dolomite with a low content (0.0%–4.0%, 1.33% on average) (Table 1), which excludes impurities. The two shale samples are also relatively pure and contain only a small amount of calcite (0.4%–1.1%, 0.75% on average) (Table 1, 2), which excludes the influence of carbonate rocks on the data. This result provides the basis for the reliability of subsequent data analysis. The $\delta^{13}C$ values of the 16 samples ranged from −0.84‰ to 0.27‰, with an average value of −0.11‰. The $\delta^{18}O$ values of all samples ranged from −10.43‰ to −9.20‰, with an average value of −9.74‰. The major and trace element content of the 16 samples showed a stable trend (Table 1, 2).

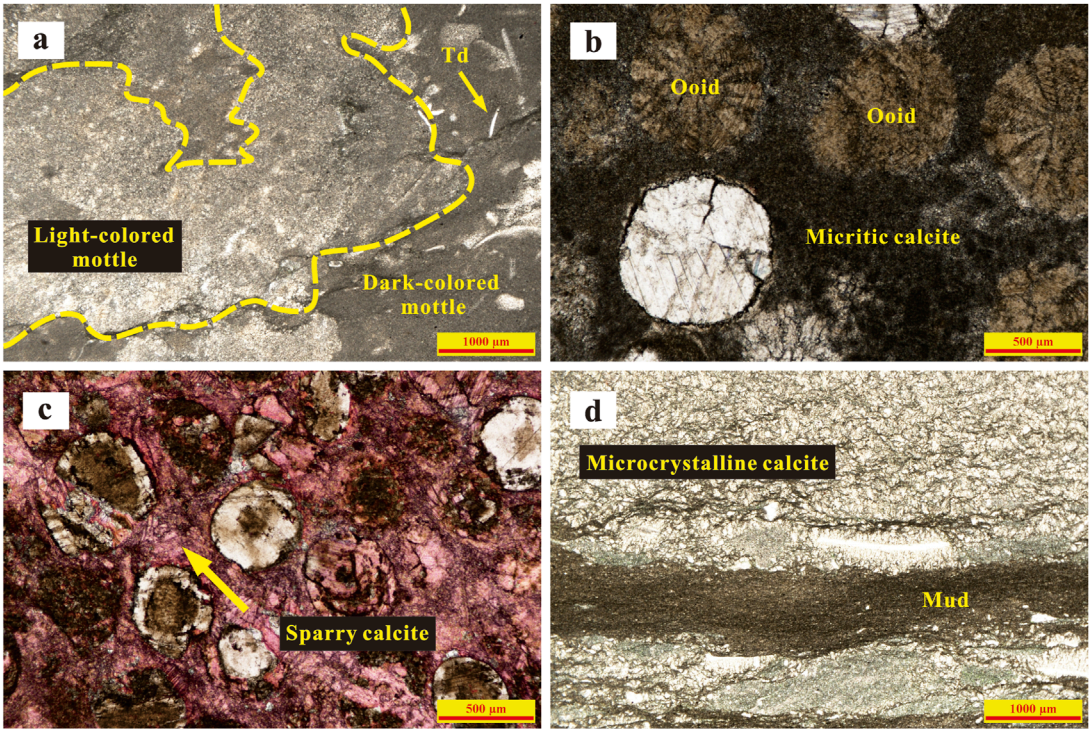

FIGURE 4
Microscopic features of rocks in Zhangxia Formation **(A)** Laminated limestone: limestone with irregular microscopic clots. The limestone is composed of micritic calcite and minor trilobite debris; **(B)** micritic oolitic limestone: The matrix among the ooids is micritic calcite; **(C)** Sparry oolitic limestone: The thin section was stained. The matrix among the ooids is sparry calcite. Dolomitization observed in some oolites' cores; **(D)** Mud-ribboned limestone: Minor trilobite debris and sporadically distributed pyrite occur. Td, Trilobite debris.

5 Discussion

5.1 Factor analysis

All the elements of the sample were subjected to R-type factor load analysis, then the elements with low load and negative correlation were removed to improve the contribution rate of the elements, and finally the elements with high load on the characteristics of the sample were screened out. The R-type factor loading matrix of the variable analysis documented a high contribution rate of $\delta^{13}C$, $\delta^{18}O$, Fe, Ti, Ni, and V contents (Figure 5), indicating a significant impact on the factor analysis results. Most of the sample information was recorded by these elements. Therefore, $\delta^{13}C$, $\delta^{18}O$, Fe, Ti, Ni, and V were selected for factor analysis to constrain the contribution rate of the eigenvalues. The Q-type factor analysis was calculated using the scatter plot established on the factor plane according to the Q-type factor loading matrix.

The variance contribution rate for the first eigenvalue was 62.46%, and the cumulative contribution rate for the second eigenvalue was 82.13% (Table 3). The eigenvalues are directly proportional to the amount of information recorded. The classification effect of samples and variables is maximized for a cumulative contribution rate of >80% (Grunsky, 2010; State, 2015). The data show that the first two eigenvalues contain the most information about the sample and its elemental composition.

Through the analysis of various elements and combined with the actual requirements, $\delta^{13}C$, $\delta^{18}O$, Fe, Ti, Ni, and V were finally selected for depositional environment analysis and used as the basis for the establishment of depositional models because they record most information of the sample (Table 3).

The planar graph of the sample data was plotted using F0 and F1 from the Q-type factor analysis. The R-type factor loading matrix (Figure 6) was projected onto the graph to obtain a scatter chart of the limestone factor analysis (Figure 7).

According to the sample characteristic index analysis results of the Q-factor analysis, the relationship of samples is classified by the similarity coefficient, and the classification pedigree diagram based on the similarity coefficient is drawn (Figure 8). To ensure the reliability of the classification, samples with a similarity of 80% were selected for classification. The samples of Zhangxia Formation can be classfied into three types: Type I is oolitic limestone; Type II is flat-pebble conglomerate; Type III includes laminated limestone, shale, and mud-ribboned limestone. The consistency of the similarity coefficient classification results with the lithology of the sample indicated that the factor analysis results were highly reliable.

TABLE 1 Geochemical data of bioherms and associated strata.

Samples no.	Lithology	Calcite	Dolomite	$\delta^{13}C_{V\text{-}PDB}$	$\delta^{18}O_{V\text{-}SMOW}$	Ca	Mn	Mg	K	Sr	Ba	Ti	Fe	Ni	V	Rb
		(%)		(‰)		(%)				(ppm)						
1	Mud-ribboned limestone	76.1	0.8	0.02	−9.29	27.33	0.05	1.24	1.06	295.0	48.6	1,656.0	10,306.0	15.8	30.6	18.7
2		81.7	0.4	−0.08	−9.79	30.82	0.11	1.88	1.14	317.0	83.8	1728.0	12,357.0	18.7	34.8	35.7
3		89.2	—	0.00	−10.12	32.95	0.15	0.16	1.48	481.0	142.0	1777.0	11,384.0	22.3	43.1	47.3
4	Sparry oolitic limestone	88.6	0.9	−0.42	−9.87	34.21	0.12	1.11	1.34	173.0	137.0	877.0	16,867.0	27.8	22.8	42.7
5		88.2	1.4	−0.41	−9.20	34.58	0.11	1.39	2.03	188.0	139.0	786.0	16,996.0	28.1	20.0	45.1
6		86.7	1.1	−0.47	−9.59	33.90	0.05	1.82	1.97	183.0	151.0	841.0	16,762.0	29.1	21.3	44.2
7	Shale	1.1	—	0.09	−9.71	4.27	0.10	1.07	1.11	408.0	123.0	1,205.0	11,043.0	22.1	42.4	39.8
8		0.4	—	0.12	−9.21	3.61	0.03	1.22	1.44	457.0	112.0	1,356.0	10,350.0	21.7	41.8	38.8
9	Laminated limestone	86.4	2.8	0.19	−9.83	26.75	0.00	4.13	0.05	75.2	12.5	1,521.0	3,107.0	8.7	27.7	0.7
10		85.4	3.4	0.22	−9.93	25.65	0.07	4.87	0.04	67.5	13.7	1,528.0	2,709.0	9.6	28.3	0.9
11		86.1	2.7	0.27	−10.43	26.51	0.02	3.79	0.09	85.1	11.4	1,554.0	2,847.0	8.9	29.7	0.6
12		85.3	4.0	0.25	−9.87	25.86	0.01	8.86	0.04	78.7	12.6	1,583.0	3,094.0	8.2	33.8	0.5
13	Flat-pebble conglomerate	85.7	0.8	−0.57	−9.88	28.24	0.02	0.51	1.12	204.0	107.0	1,088.0	15,374.0	25.7	26.7	34.0
14		82.6	—	−0.84	−9.52	32.99	0.06	0.44	1.53	196.0	115.0	1,074.0	16,124.0	28.1	25.8	36.0
15	Micritic oolitic limestone	82.2	—	−0.06	−9.86	40.10	0.08	0.65	0.39	356.0	60.4	924.0	6,897.0	15.8	20.5	15.4
16		82.9	0.3	−0.03	−9.74	40.33	0.03	1.91	1.8	447.0	91.6	999.0	9,487.0	18.0	21.2	36.5

10.3389/feart.2024.1433182

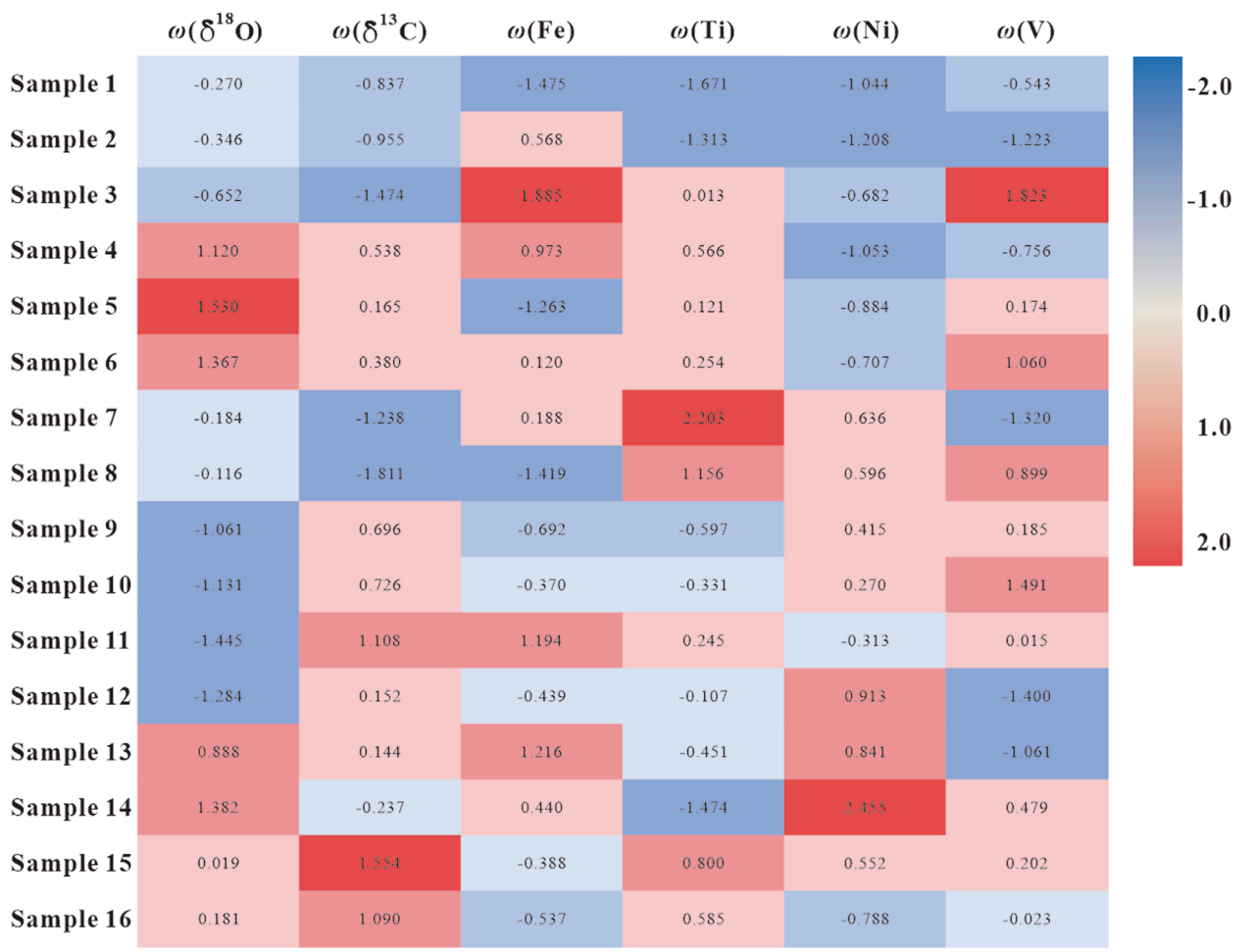

FIGURE 5
Heatmap of Q-type factor score matrix.

5.2 Depositional environments based on regional depositional background and characteristics

The presence of trilobite fossils in the bioherm indicates good water circulation. The growth of microorganisms requires appropriate paleotemperature, suitable paleosalinity, good sunshine conditions, and an adequate supply of organic matter. Therefore, the depositional environment of the bioherm was a relatively deep-water environment with weak hydrodynamics. The color of the shale around the bioherm was dark green, indicating that the shale was also deposited in a relatively deep-water environment with weak hydrodynamics. According to the geological background, the depositional environment of the bioherm and shale is the transition environment from deep water to shallow water at the edge of the carbonate platform.

In the bottom strata of the bioherm, flat-pebble conglomerates were disordered, indicating short-term storm deposition during this period. Micritic oolitic limestone is filled with micritic calcite, and the granularity of the ooid is uniform, the color is gray or light gray, The granularity of the ooids in micritic oolitic limestone is uniform. The filling among the ooids was micritic calcite (Figure 4B). This phenomenon shows that although the ooid formed in a turbulent shallow-water environment, the micritic oolitic limestone formed in a weak hydrodynamic environment.

The oolitic interstitials of the sparry oolitic limestone were filled with sparry calcite (Figure 4C), indicating that the sparry oolitic limestone developed in a relatively shallow-water environment above the fair-weather wave base. The mud-ribboned limestone may have formed in an open platform according to the sequence.

5.3 Depositional environments based on geochemical analysis

This paper analyzed high-impact element data from factor analysis to determine paleotemperature, paleosalinity, paleoredox, paleodepth, etc. However, after sediment deposition, it undergoes a long diagenetic process, which is a complex geological process and has many influences on rock composition. Different diagenetic processes interact and influence each other to determine the final composition and properties of rocks (Zhu, 2008; Matthew and Max, 2024). Therefore, before analysis, it is necessary to

TABLE 2 Average geochemical values of bioherms and associated strata.

Lithology	Calcite (%)	Dolomite (%)	$\delta^{13}C_{V\text{-}PDB}$ (‰)	$\delta^{18}O_{V\text{-}SMOW}$ (‰)	Ca (%)	Mn (%)	Mg (%)	K (%)	Sr (ppm)	Ba (ppm)	Ti (ppm)	Fe (ppm)	Ni (ppm)	V (ppm)	Rb (ppm)
Mud-ribboned limestone	82.33	0.40	−0.02	−9.73	30.37	0.10	1.09	1.23	364.3	91.5	1720.3	11,349.0	18.9	36.17	33.9
Sparry oolitic limestone	87.83	1.13	−0.43	−9.55	34.23	0.09	1.44	1.78	181.3	142.3	834.7	16,875.0	28.3	21.37	44.0
Shale	0.75	—	0.11	−9.46	3.94	0.07	1.15	1.28	432.5	117.5	1,280.5	10,696.5	21.9	42.1	39.3
Laminated limestone	85.80	3.23	0.23	−10.01	26.19	0.03	5.41	0.06	76.6	12.6	1,546.5	2,939.3	8.9	29.9	0.7
Flat-pebble conglomerate	84.15	0.40	−0.71	−9.70	30.62	0.04	0.48	1.33	200.0	111.0	1,081.0	15,749.0	26.9	26.3	35.0
Micritic oolitic limestone	82.55	0.15	−0.05	−9.80	40.22	0.06	1.28	1.10	401.5	76.0	961.5	8,192.0	16.9	20.9	26.0

reduce the impact of diagenesis on the data and confirm that the sample retains the original geochemical composition at the time of deposition. Previous studies have shown that long-term variations in the $\delta^{13}C$ isotope compositions of marine carbonate rocks can accurately characterize changes in paleoenvironments and bio-events (Brasier et al., 1994; Ishikawa et al., 2014). The academic community considers data with $\delta^{18}O > -10‰$ reliable (Kaufman and Knoll, 1995; Zhu et al., 2004; Li et al., 2009). However, oxygen isotope values below −10‰ do not necessarily correspond to invalid data for carbon isotopes, as carbon isotopes in carbonates exhibit better resistance to later modifications than oxygen isotopes in the context of atmospheric freshwater and hydrothermal processes (Anderson and Arthur, 1983; Glumac and Spivak-Birndord, 2002). Therefore, even if $\delta^{18}O$ is less than −10‰, the $\delta^{13}C$ may still be valid.

The $\delta^{13}C$ and $\delta^{18}O$ datasets do not show a clear linear correlation (Figures 9, 11A). The lack of a positive correlation between carbon and oxygen isotopes in carbonate rock samples indicates that the original carbon-oxygen isotope features were preserved (Kaufman et al., 1991; Derry et al., 1992; Dilliard et al., 2007; Wotte et al., 2007). Furthermore, the $\delta^{13}C$ values in the surrounding areas exhibited a similar curve shape and evolutionary trend to the $\delta^{13}C$ values in this study. In conclusion, the data for carbon and oxygen isotopes were reliable.

5.3.1 Paleosalinity

Previous studies have shown that the carbon and oxygen isotope compositions of carbonate rocks are affected by the salinity of water, and the $\delta^{18}O$ value has a positive correlation with salinity. Keith and Weber (1964) proposed an empirical formula using $\delta^{13}C$ and $\delta^{18}O$ values to calculate the salinity index Z of depositional media:

$$Z = 2.048 \times (\delta^{13}C + 50) + 0.498 \times (\delta^{18}O + 50)$$

The Z value is not the exact salinity value, but is positively correlated with paleosalinity. Z values of less than 120 indicate a freshwater environment, Z values greater than 120 indicate a seawater environment, and Z values increase with increasing paleosalinity (Keith and Weber, 1964).

Experimental data show that the Z value ranges from 120.84‰ to 122.96‰, with an average value of 122.23‰ (Figure 9). The salinity of seawater is relatively low and does not change significantly overall. The salinity of flat-pebble conglomerate and sparry oolitic limestone was significantly lower than that of laminated limestone and shale.

Shallow water environments are more susceptible to atmospheric precipitation, resulting in lower salinity than deep-water environments. The difference in salinity also indicates that the paleodepth of conglomerate and oolitic limestone is shallower than that of dolomite limestone and shale.

5.3.2 Paleotemperature

Temperature also affects the carbon and oxygen isotopic composition of carbonate rocks, which is mainly reflected in the effect on $\delta^{18}O$ (Li et al., 2014). Previous studies have found that when the salinity of the medium remains unchanged, the higher the temperature, the lower the $\delta^{18}O$ value. Therefore, the $\delta^{18}O$ value can be a relatively reliable indicator for restoring ancient temperatures.

For older rocks, such as Cambrian carbonates, $\delta^{18}O$ values must be dated before calculation (Shao and Jones, 1999).

TABLE 3 Contribution rates of factor analysis eigenvalues.

Eigenvalue variance	Eigenvalue	Contribution	Cumulative contribution
λ_1	56.210	62.46%	62.46%
λ_2	17.708	19.68%	82.13%
λ_3	10.811	12.01%	94.14%
λ_4	3.970	4.41%	98.55%
λ_5	1.173	1.30%	99.86%
λ_6	0.128	0.14%	100.00%

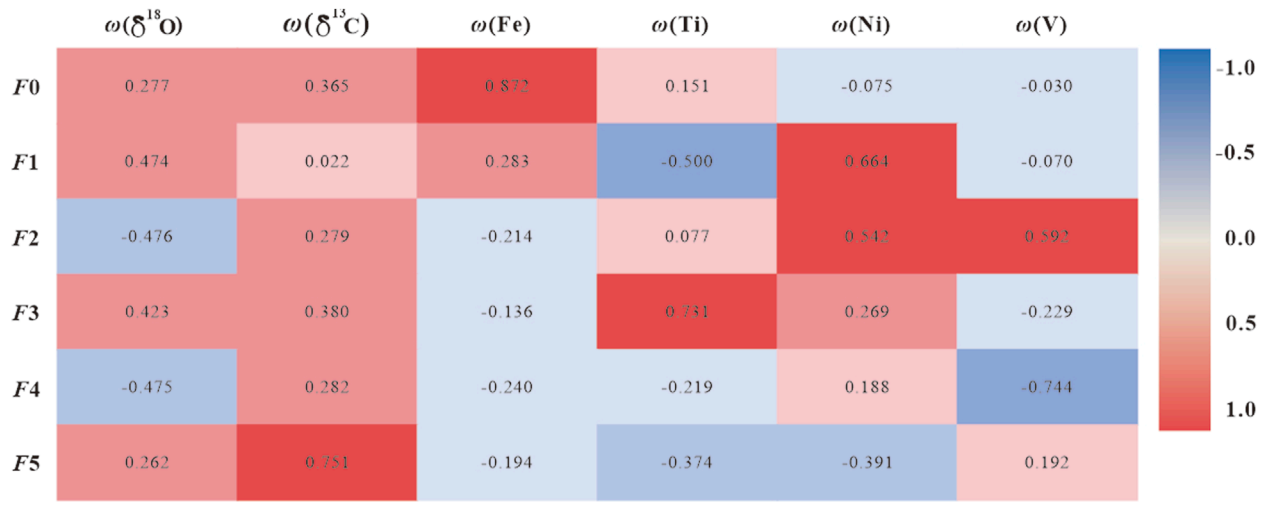

FIGURE 6
Heatmap of R-type factor loading matrix.

The $\delta^{18}O$ values of Quaternary Marine carbonate rocks were calibrated with an average $\delta^{18}O$ value of-1.2‰ as the standard (Shao et al., 1996; Meng et al., 2016). The $\Delta\delta^{18}O$ values of each group can be obtained by subtracting the average $\delta^{18}O$ values of each group from the average $\delta^{18}O$ values of Quaternary Marine carbonate rocks (−1.2‰), and then subtracting the measured values of each sample from their $\Delta\delta^{18}O$ values, the correction values of $\delta^{18}O_{CaCO3}$ in the formula can be obtained.

In this study, the formula proposed and corrected by previous researchers was used to calculate the ancient temperature (Chen et al., 2012; Luo et al., 2013):

$$T = 16.9 - 4.2 \times (\delta^{18}O_{CaCo3} + 0.22) + 0.13 \times (\delta^{18}O_{CaCo3} + 0.22)^2$$

The calculated results show that the temperature of the Zhangxia Formation ranges from 18.63°C to 24.13°C, with an average of 21.01°C (Figure 9). The temperature occasionally changed, but the change was small, and the overall temperature was stable and suitable.

5.3.3 Paleodepth

Carbon isotopes in marine carbonate rocks are closely related to organic carbon burial rates (Huang, 1997). The $\delta^{13}C$ value of carbonate rocks is positively correlated with the change in sea level (Tian and Zeng, 1995; Shao and Jones, 1999). With the rise in sea level, the water body gradually deepens, the organic carbon burial rate increases, photosynthesis weakens, oxygen consumption increases, and organic carbon in the ocean decreases, increasing $\delta^{13}C$ content. Conversely, when the sea level falls, the $\delta^{13}C$ content decreases. Carbon isotopes are weakly affected by diagenesis and preserve the original isotope information; therefore, it is a reliable method to restore the paleodepth of marine strata based on carbon isotopes. Data show that sea level change in the Zhangxia Formation is characterized by alternating deep and shallow (Figure 9). Sea level decreased during the deposition period of flat-pebble conglomerate and sparry oolitic limestone. Changes in sea level are consistent with paleosalinity records.

The threshold of paleodepth index established by previous studies may not accurately reflect the actual situation, but the

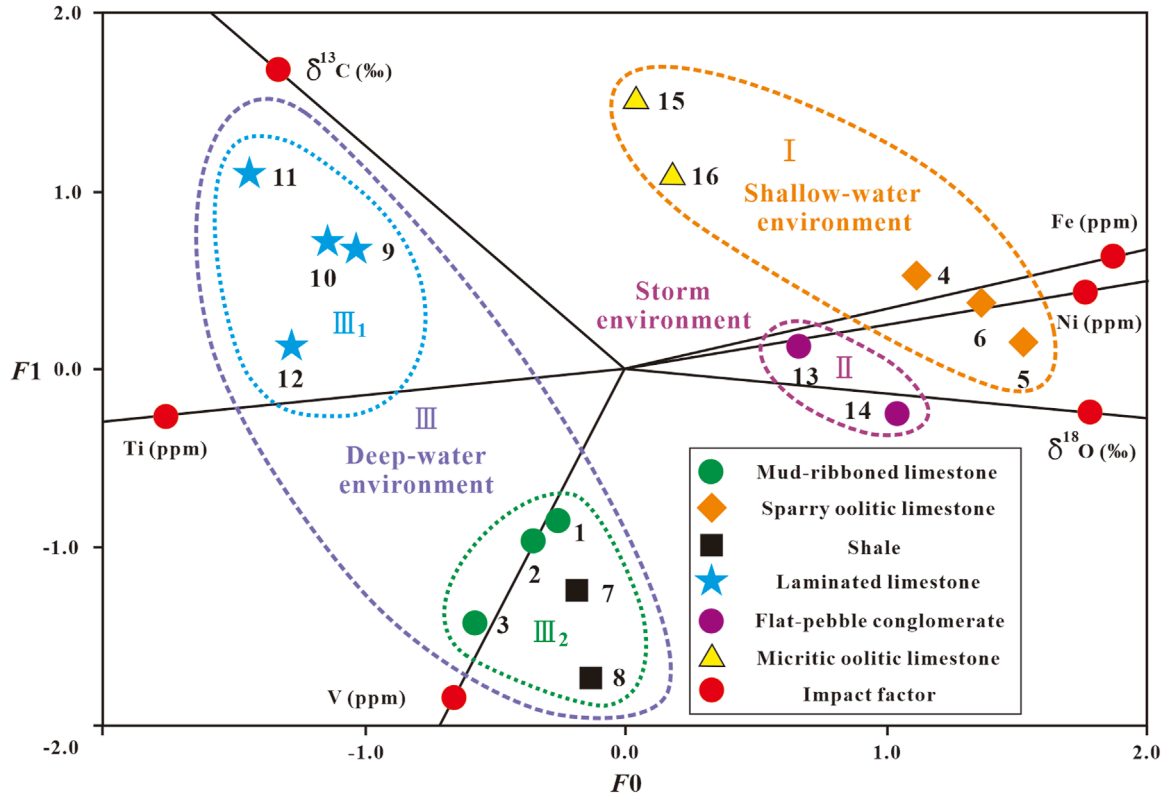

FIGURE 7
Principal factor, cluster analysis, and system tract partition diagram.

degree of anoxia can be inferred by analyzing the relative difference of several indicators (Rimmer, 2004; Francisco and Laura, 2011), and thus the change in paleodepth can be inferred. In this paper, V/Ni and V/(V+Ni) are used to represent palaeodepth change. V and Ni mainly exist in terrigenous detrital and clay minerals. The energy of seawater in a coastal environment is higher, the detrital content is lower, and the mass fractions of V and Ni are lower. However, the deep-water environment is quiet and conducive to the deposition of terrigenous materials. Therefore, the V/Ni value in a deep-water environment is higher than that in a shallow-water environment (Hu, 1994), and the V/Ni value increases with increasing water depth (Xu et al., 2017). Therefore, an increase in the V/Ni value indicates that the water body deepens, and *vice versa*. Notably, the V/Ni value of the bioherm is higher than that of shale, not because of differences in water depth, but because microorganisms capture suspended debris and clay as they grow. Additionally, V/(V+Ni) can indirectly reflect changes in paleodepth by indicating redox conditions: In an anoxic reducing environment in deep water, V/(V+Ni) is greater than 0.84; In a less stratified anoxic or suboxic environment, the V/(V+Ni) value ranges from 0.60 to 0.84; representing a transitional environment from deep to shallow water; In an oxidizing environment of shallow water or exposure conditions, V/(V+Ni) is less than 0.60 (Patterson et al., 1986; Dill et al., 1988).

The V/Ni of flat-pebble conglomerate ranges 0.92~1.04, with an average value of 0.98; laminated limestone ranges 2.95~4.12, with an average value of 3.40. The V/(V+Ni) of flat-pebble conglomerate values range 0.48~0.51, with an average value of 0.49; laminated limestone range 0.75~0.80, with an average value of 0.77.

V/Ni and V/(V+Ni) values for other types of rocks are between flat-pebble conglomerate and laminated limestone. Simultaneous V/Ni and V/(V+Ni) changes indicate flat-pebble conglomerates developed in shallow or exposed environments, bioherms developed in deep water environments, and other rock types developed in transitional environments (Figure 9). Paleodepth also showed alternating depths consistent with sea level change, indicating that the study area may have been an open platform during this period.

5.3.4 Paleoredox

Differences in the occurrence state and enrichment of variable valence elements (U, V, Mo, Cu, Fe, etc.) under different redox conditions can be used to infer changes in the redox state of a water body during sediment deposition (Hatch and Leventhal, 1992). The relationship between V and Ni can also be used as an indicator to determine the oxidation-reduction environment of the depositional medium (Rimmer, 2004; Brumsack, 2006; Tribovillard et al., 2006).

Fe is easily reduced, while Ti is more easily oxidized (Ronald and Carol, 2013; El Attar and Pranter, 2016). Based on the contrasting characteristics of Fe and Ti, Fe/Ti can be used as an index to judge the REDOX condition of the depositional environment. Fe/Ti has a low value in reducing environments but a high value in oxidizing environments. Coherence between REDOX (Fe/Ti) and paleodepth (V/Ni) indices indicates that bioherms and shales

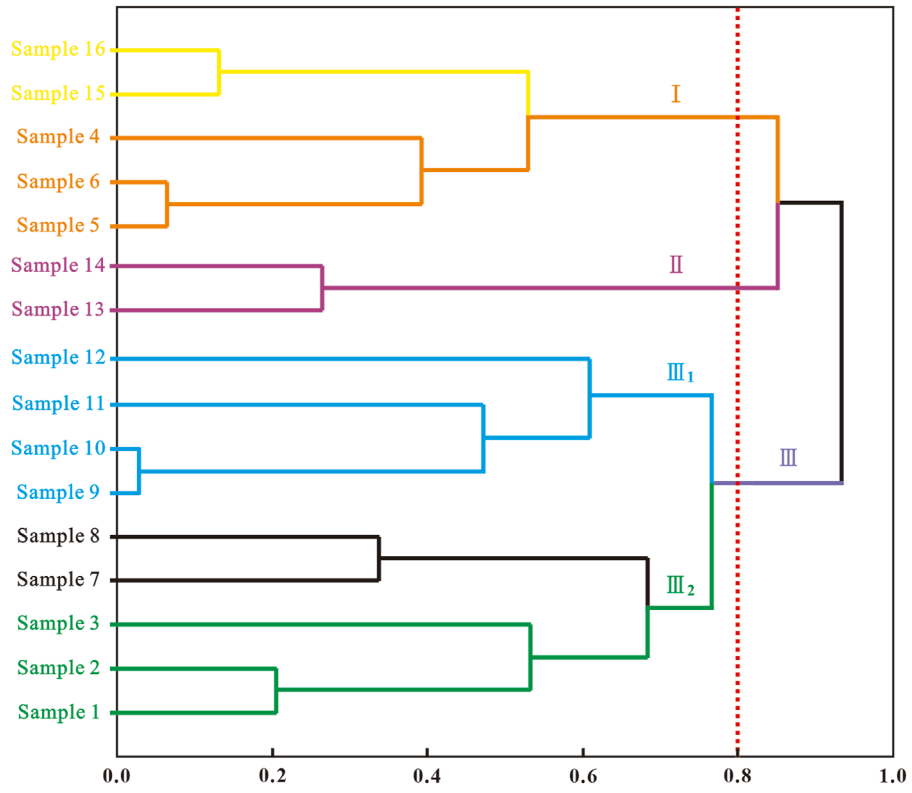

FIGURE 8
Classification pedigree diagram based on similarity coefficient.

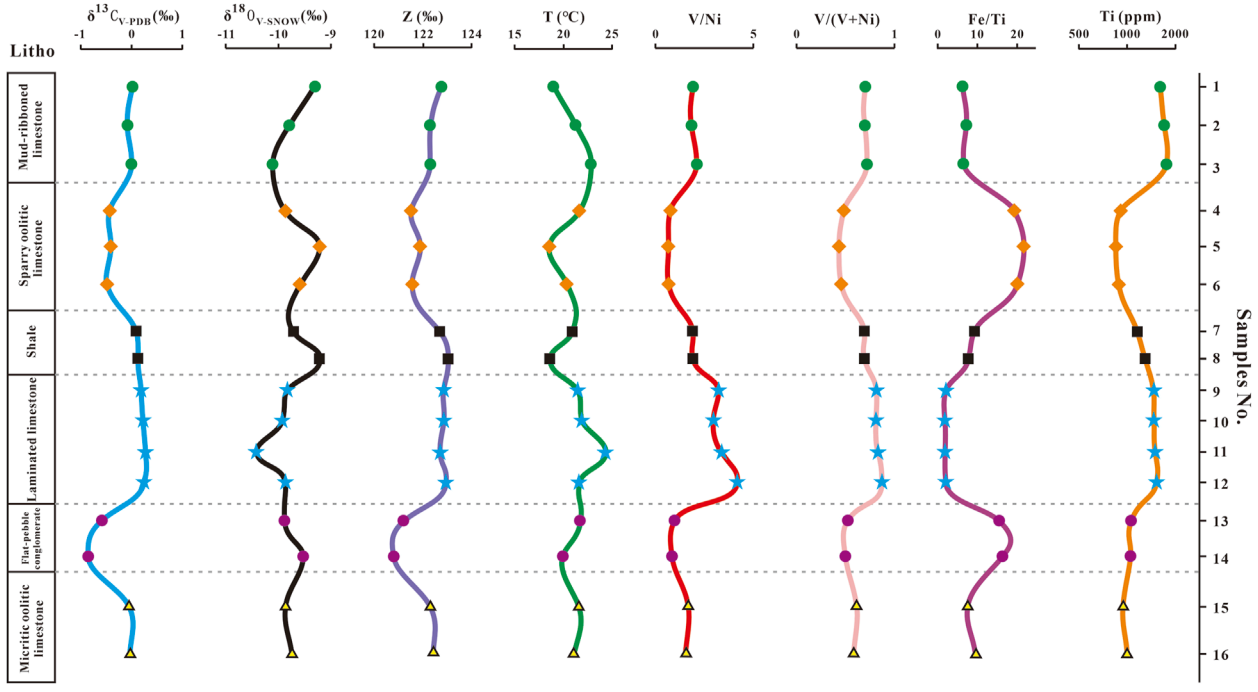

FIGURE 9
Line graph of $\delta^{13}C$, $\delta^{18}O$, and element content ratio.

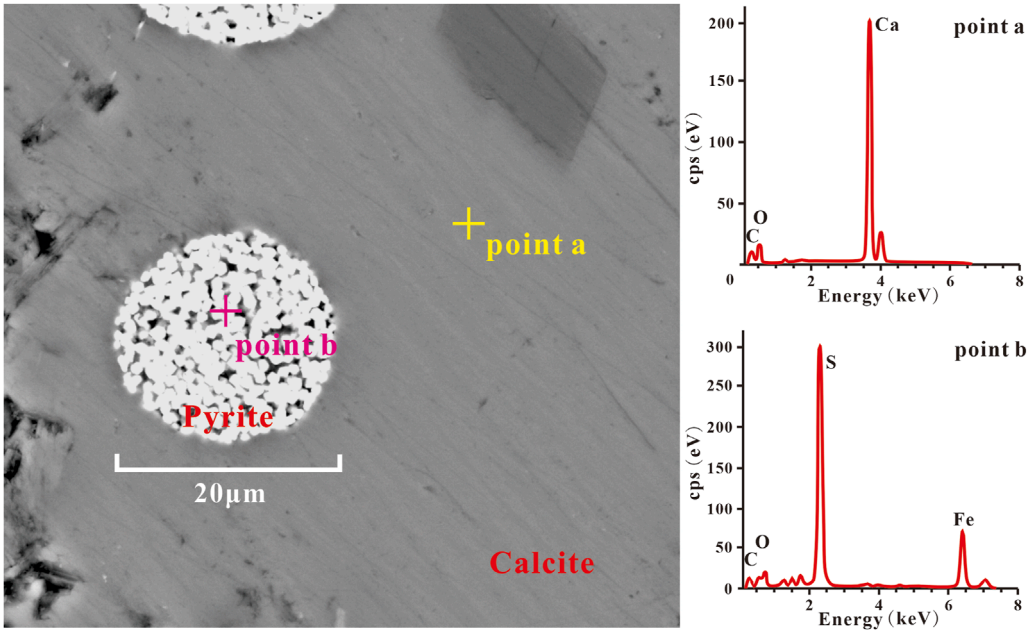

FIGURE 10
SEM image of framboidal pyrite aggregates in the bioherm. The phase EDS spectrum shows strong peaks for S Ka and Fe Ka, indicating high amounts of S and Fe, and identifies the phase as pyrite.

developed in a reduced environment. At the same time, the flat-pebble conglomerates and sparry oolitic limestones were deposited in an oxidizing environment and their REDOX properties were mainly controlled by water depth (Figure 9).

A small amount of pyrite framboids was found in the bioherm. Pyrite framboids are a common form of pyrite found in sedimentary rocks (Large et al., 1999) and usually indicate oxygen-depleted environments (Bond and Wignall, 2010). Pyrite framboids are preserved in the early diagenetic stage (Shevelkova et al., 1996), and their microcrystalline structure does not change with depositional environments (Wilkin and Barnes, 1997; Grimes et al., 2001). Therefore, the size and shape of pyrite framboid aggregates are reliable indicators of oxygen content and water salinity during deposition (Berner, 1984; Shevelkova et al., 1996). SEM images of bioherm samples show that individual pyrite crystals have a size of about 5 μm while the diameter of the aggregates is up to 20 μm (Figure 10), indicating reducing conditions during deposition. This further supports the idea that bioherms develop in a reduced environment.

5.3.5 Terrigenous input

Elements enriched in terrigenous detritus typically increase with increasing terrigenous inputs (Kryc et al., 2003; Tribovillard et al., 2006). Ti, Al and Si in marine sedimentary rocks are mainly derived from terrigenous detritus, and their contents are controlled by continental weathering (Tribovillard et al., 2006). However, Al and Si content may also be influenced by biological processes and hydrothermal fluids. Therefore, Ti was used to characterize the input of terrigenous detritus. The fluctuation of Ti content in the study area during the deposition period was slight, indicating that the terrigenous input was stable. The terrestrial input in the bioherms and shale is higher than that in the oolitic limestones and flat-pebble conglomerates, which provide sufficient nutrients for the growth of microorganisms. Terrigenous input and paleodepth varied simultaneously (Figure 9), further indicating that bioherms developed in the open platform.

5.4 Relationship between various environmental factors

The paleoenvironment is an organic whole, and there is a specific coupling relationship among paleoenvironmental elements, such as paleoclimate, paleosalinity, paleotemperature, and paleodepth. When one element changes, it inevitably causes a series of chain changes in other elements (Fairbridge, 1981; Yang, 2004; Wang et al., 2016). Changes in the paleoenvironment inevitably lead to changes in the depositional environment and the characteristics of sediments formed in this environment. The paleoenvironment plays a controlling role in sedimentation. Different paleoenvironmental factors formed different sedimentary facies, and different sedimentary facies have different paleoenvironmental attributes (Jiang, 2010).

To further verify the relationship between the various paleoenvironmental elements, an intersection scatter plot was drawn, and the correlation coefficient (R^2) was calculated to determine the correlation between them. Fe/Ti, V/Ni, and Ti from samples in the study area showed a strong linear relationship (Figures 11B–D), indicating that paleodepth and paleoredox levels in the study area were strongly correlated with

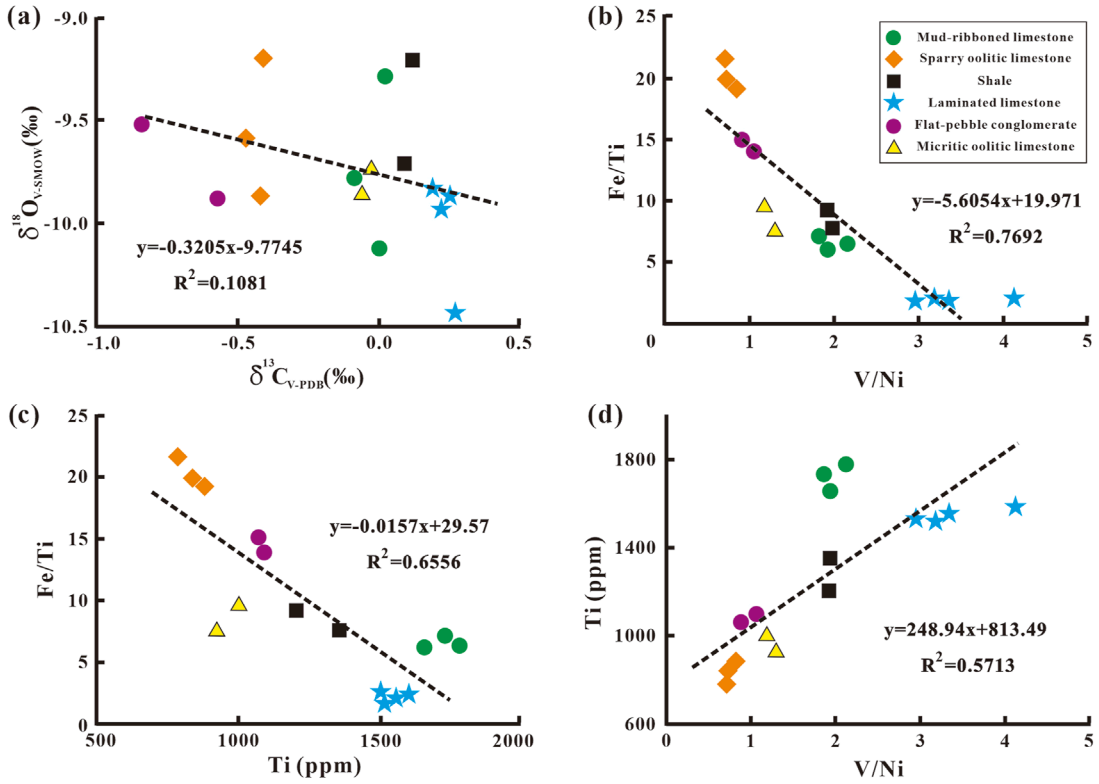

FIGURE 11
Plots of **(A)** $\delta^{13}C$ versus $\delta^{18}O$, **(B)** V/Ni versus Fe/Ti, **(C)** Ti versus Fe/Ti, and **(D)** V/Ni versus Ti.

terrigenous input. The paleoenvironmental elements indicated by the geochemical characteristics of the elements in the study area have good integrity and correlation, which jointly control the rock characteristics of Zhangxia Formation. This provides a basis for the depositional environment of the study area to be an open platform.

5.5 Reconstruction of paleoenvironments and depositional model

The depositional environment of Zhangxia Formation in the study area is characterized by low oxygen, high temperature, and low salinity, with stable terrigenous input. Based on the classification results from the sample similarity coefficient (Figure 8), the distribution of sample factors was divided, revealing the correlation between sample types and influencing factors (Figure 7).

According to the classification, Type I (oolitic limestone) samples were deposited in shallow water environments. These environments are often associated with high hydrodynamic forces, high terrigenous input, and strong oxidation. Consequently, data points for Type I primarily cluster around axes representing oxidation-sensitive factors such as Fe and Ni (Figure 7).

Type II samples (flat-pebble conglomerates) represent storm deposits characterized by strong hydrodynamics, shallow depth, high oxidation, and low source supply. Although the storm environment during the deposition of flat-pebble conglomerate is an oxidizing environment like shallow water, it exhibits lower temperature and salinity. Therefore, compared to Type I, Type II samples are more aligned with the temperature- and salinity-related axis of the factor $\delta^{18}O$, and their correlation with Fe and Ti is weaker (Figure 7).

Type III samples developed in a deep-water environment with greater depth, stronger reducing conditions, higher salinity, and significant source input. Data points for this sample type are concentrated along the $\delta^{13}C$, Ti, and V axes, which are related to factors such as water depth, salinity, and terrigenous input (Figure 7). Type III samples can be further subdivided into two categories: Type III_1 samples are laminated limestone, where microbial growth has a regulating effect on seawater salinity, making salinity-related $\delta^{13}C$ their main characteristic compared with III_2. Type III_2 samples are shales and mud-ribboned limestone, where water depth is the primary control factor. Consequently, compared to Type III_1, Type III_2 samples are more aligned with the depth-related V axis (Figure 7).

Combined with the Sequence stratigraphy geological background of the study area, it is believed that the rocks in the

10.3389/feart.2024.1433182

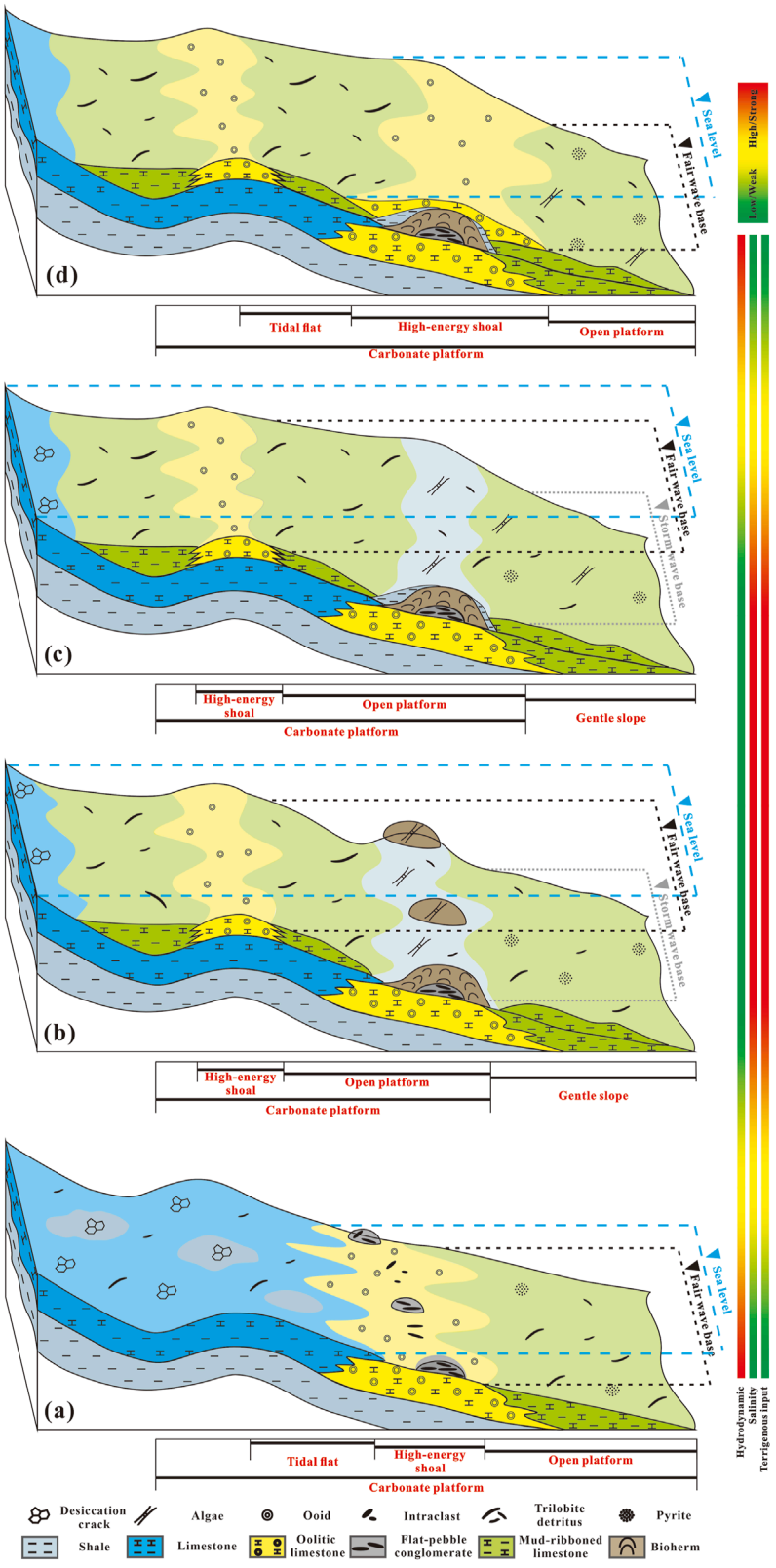

FIGURE 12
Model of bioherm deposition in Zhangxia Formation, Miaolingian, Cambrian. Environment and water depth for the development of **(A)** flat-pebble conglomerates; **(B)** bioherms; **(C)** shales; **(D)** sparry oolitic limestones.

study area were deposited on the open platform at the edge of the carbonate platform, and the water depth changed frequently. On this basis, a depositional model of bioherm in Zhangxia Formation was proposed.

In the early stages of sedimentation, oolites were formed in environments with low sea level and strong hydrodynamics, and the study area was located above the fair-wave base. As sea level rises, the study area drops below the fair-wave base, reducibility is enhanced, hydrodynamic energy is weakened, and oolites begin to deposit. Due to the weak water energy at this time, the space between the oolites is filled by micrite calcite, forming micrite oolitic limestone.

Later, storm events caused sea level to drop rapidly to the base of the storm-wave base, exposing the area to the surface. During this period, water was high energy and oxidizing, with low salinity and limited terrigenous input. The storm brought pebbles, which accumulated to form flat-pebble conglomerates (Figure 12A). In the following stage, as sea level rose again, the area was submerged below the fair-wave base, water energy and oxidation decreased further, and salinity and terrigenous input increased. Conditions in the area—including salinity, temperature, sunlight, oxidation, and nutrient input—became conducive to microbial growth. Microbes proliferated over flat-pebble conglomerates, trapping and binding calcium carbonate to form mound-like carbonate structures, known as bioherms (Figure 12B).

In areas lacking the flat-pebble conglomerate, microbial communities could not establish, so instead of bioherms, shale developed from muddy deposits encased bioherms (Figure 12C). During the late bioherm development phase, sea levels declined, raising the study area above the fair-wave base. Increased water energy and oxidation, combined with reduced salinity and terrigenous input, created conditions unsuitable for microbial survival, causing bioherm growth to stop. Sparry oolitic limestone, formed under high energy conditions, then overlaid the bioherms and surrounding shale (Figure 12D). Towards the final stage, frequent sea level fluctuations led to unstable shifts in salinity, oxidation, and terrigenous input, resulting in alternating deposits of mud and calcite that formed mud-ribboned limestone.

6 Conclusion

The rocks in the study area were deposited on an open platform at the edge of the carbonate platform, and the water depth frequently changed. The study area is mainly a shallow-water environment with low oxygen, high temperature, and low salinity. Temperature, salinity, oxidation, water depth, and light conditions are ideal, and terrigenous inputs are sufficient. This environment is suitable for the growth of microorganisms; therefore, bioherms begin to develop. As the water depth becomes shallow, the water and nutrient conditions are no longer ideal for the growth of microorganisms, and bioherms stop developing.

The factors selected from geochemical elements through factor analysis can characterize most of the overall features. The sample correlation shown by the selected elements also allows a reliable classification of samples. Therefore, the method based on factor analysis for the deposition model is not only feasible, but also effectively avoids the ambiguity and multi-solution of traditional methods.

Data availability statement

The original contributions presented in the study are included in the article/Supplementary Material, further inquiries can be directed to the corresponding author.

Author contributions

HC: Writing–original draft, Writing–review and editing, Conceptualization, Data curation, Methodology, Project administration, Resources. ZJ: Writing–original draft, Writing–review and editing, Conceptualization, Data curation, Methodology, Project administration, Resources. RZ: Writing–original draft, Writing–review and editing, Conceptualization, Data curation, Methodology, Project administration, Resources. JW: Writing–original draft, Writing–review and editing, Conceptualization, Funding acquisition, Methodology, Project administration, Resources. XZ: Writing–original draft, Writing–review and editing, Conceptualization, Funding acquisition, Methodology, Project administration, Resources. BL: Writing–review and editing, Investigation, Project administration, Visualization. YB: Writing–review and editing, Investigation.

Funding

The author(s) declare that financial support was received for the research, authorship, and/or publication of this article. This study was supported by the National Natural Science Foundation of China (Grant No. 41872018).

Conflict of interest

Authors HC and RZ were employed by CNPC. Author XZ was employed by CNOOC Research Institute Co. Ltd.

The remaining authors declare that the research was conducted in the absence of any commercial or financial relationships that could be construed as a potential conflict of interest.

Publisher's note

Supplementary material

The Supplementary Material for this article can be found online at: https://www.frontiersin.org/articles/10.3389/feart.2024.1433182/full#supplementary-material

References

Aksu, A. E., Hiscott, R. N., Kostylev, V. E., and Yaltırak, C. (2018). Organized patches of bioherm growth where the strait of dardanelles enters the marmara sea, Turkey. *Palaeogeogr. Palaeoclimatol. Palaeoecol.* 490 (1), 325–346. doi:10.1016/j.palaeo.2017.11.010

Algeo, T. J., and Maynard, J. B. (2004). Trace-element behavior and redox facies in core shales of Upper Pennsylvanian Kansas-type cyclothems. *Chem. Geol.* 206, 289–318. doi:10.1016/j.chemgeo.2003.12.009

Alhija, F. A. N. (2010). "Factor analysis: an overview and some contemporary advances," in *International encyclopedia of education*. Third Edition (Elsevier).

Anderson, T. F., and Arthur, M. A. (1983). Stable isotopes of oxygen and carbon and their application to sedimentology and palaeoenvironmental problems. *Soc. Econ. Palaeontol. Mineralogists* 10, 155–159. doi:10.2110/scn.83.01.0000

Berner, R. A. (1984). Sedimentary pyrite formation: an update. *Geochimica Cosmochimica Acta* 48, 605–615. doi:10.1016/0016-7037(84)90089-9

Bhat, G. M., Craig, J., Hafiz, M., Hakhoo, N., Thurow, J. W., Thusu, B., et al. (2012). Geology and hydrocarbon potential of neoproterozoic–cambrian basins in asia: an introduction. *Geol. Soc. Lond. Spec. Publ.* 366, 1–17. doi:10.1144/SP366.15

Bond, D., and Wignall, P. B. (2010). Pyrite framboid study of marine Permian-Triassic boundary sections: a complex anoxic event and its relationship to contemporaneous mass extinction. *Geol. Soc. Am. Bull.* 122, 1265–1279. doi:10.1130/B30042.1

Bosak, T., Knoll, A. H., and Petroff, A. P. (2013). The meaning of stromatolites. *Annu. Rev. Earth Pl. S. C.* 41, 21–44. doi:10.1146/annurev-earth-042711-105327

Bourillot, R., Vennin, E., Kolodka, C., Rouchy, J. M., Caruso, A., Durlet, C., et al. (2009). The role of topography and erosion in the development and architecture of shallow-water coral bioherms (Tortonian-Messinian, Cabo de Gata, SE Spain). *Palaeogeogr. Palaeoclimatol. Palaeoecol.* 281, 92–114. doi:10.1016/j.palaeo.2009.07.015

Brasier, M. D., Corfield, R. M., Derry, L. A., and Zhuravlev, A. Y. (1994). Multiple $d^{13}C$ excursions spanning the Cambrian explosion to the Botomian crisis in Siberia. *Geology* 22, 455. doi:10.1130/0091-7613(1994)022<0455:MCESTC>2.3.CO;2

Brumsack, H. J. (2006). The trace metal content of recent organic carbon-rich sediments: implications for Cretaceous black shale formation. *Palaeogeogr. Palaeoclimatol. Palaeoecol.* 232, 344–361. doi:10.1016/j.palaeo.2005.05.011

Calvert, S. E., and Pedersen, T. F. (1993). Geochemistry of recent oxic and anoxic marine sediments: implications for the geological record. *Mar. Geol.* 113, 67–88. doi:10.1016/0025-3227(93)90150-t

Chen, Q., Zhang, H. Y., Li, W. H., Hao, S. L., and Liu, Z. (2012). Characteristics of carbon and oxygen isotopes of the Ordovician carbonate rocks in ordos and their implication. *J. Palaeogeogr. Chin. Ed.* 14 (1), 117–124. doi:10.1007/s11783-011-0280-z

Chough, S. K., Lee, H. S., Woo, J., Chen, J., Choi, D. K., Lee, S., et al. (2010). Cambrian stratigraphy of the North China platform: revisiting principal sections in shandong province, China. *Geosciences J.* 14, 235–268. doi:10.1007/s12303-010-0029-x

Colodner, D., Sachs, J., Ravizza, G., Turekian, K., Edmond, J., and Boyle, E. (1993). The geochemical cycle of rhenium: a reconnaissance. *Earth Planet. Sci. Lett.* 117, 205–221. doi:10.1016/0012-821x(93)90127-u

Crusius, J., Calvert, S., Pedersen, T., and Sage, D. (1996). Rhenium and molybdenum enrichments in sediments as indicators of oxic, suboxic and sulfidic conditions of deposition. *Earth Planet. Sci. Lett.* 145, 65–78. doi:10.1016/S0012-821X(96)00204-X

Derry, L. A., Kaufman, A. J., and Jacobsen, S. B. (1992). Sedimentary cycling and environmental change in the Late Proterozoic: evidence from stable and radiogenic isotopes. *Geochimica Cosmochimica Acta* 56, 1317–1329. doi:10.1016/0016-7037(92)90064-P

Dill, H., Teschner, M., and Wehner, H. (1988). Petrography, inorganic and organic geochemistry of Lower Permian carbonaceous fan sequences ("Brandschiefer Series") — Federal Republic of Germany: constraints to their paleogeography and assessment of their source rock potential. *Chem. Geol.* 67 (3/4), 307–325. doi:10.1016/0009-2541(88)90136-2

Dilliard, K. A., Pope, M., Coniglio, M., Hasiotis, S., and Lieberman, B. (2007). Stable isotope geochemistry of the lower Cambrian Sekwi Formation, Northwest Territories, Canada: implications for ocean chemistry and secular curve generation. *Palaeogeogr. Palaeoclimatol. Palaeoecol.* 256, 174–194. doi:10.1016/j.palaeo.2007.02.031

Du, F. P., Yang, J. Y., Zhao, X. C., He, X. Y., Zhang, P., Zhang, J. Y., et al. (2024). Characteristics and paleoenvironmental indications of caddisfly larval cases-stromatolite bioherms in the Lower Cretaceous in Liupanshan Basin, Central China. *Cretac. Res.* 165, 105973. doi:10.1016/j.cretres.2024.105973

El Attar, A., and Pranter, M. J. (2016). Regional stratigraphy, elemental chemostratigraphy, and organic richness of the niobrara member of the mancos shale, piceance basin, Colorado. *Am. Assoc. Pet. Geol. Bull.* 100, 345–377. doi:10.1306/12071514127

Erickson, B. E., and Helz, G. R. (2000). Molybdenum(VI) speciation in sulfidic waters:. *Geochimica Cosmochimica Acta* 64, 1149–1158. doi:10.1016/S0016-7037(99)00423-8

Everitt, B., and Hothorn, T. (2011). "Cluster analysis," in *An introduction to applied multivariate analysis with R. Use R* (New York, NY: Springer). doi:10.1007/978-1-4419-9650-3_6

Fairbridge, R. W. (1981). Holocene wiggles. *Natrue* 292, 670–671. doi:10.1038/292670a0

Filzmoser, P., Hron, K., Reimann, C., and Garrett, R. (2009). Robust factor analysis for compositional data. *Comput. and Geosciences* 35, 1854–1861. doi:10.1016/j.cageo.2008.12.005

Francisco, S., and Laura, L. K. (2011). Análisis geoquímico (elementos mayores, menores, traza, $\delta^{13}c$, $\delta^{18}o$ y tierras raras) de microbialitas selectas provenientes de la formación san casiano (triásico medio-superior, ne de italia). *Boletn De. La Soc. Geolgica Mex.* 63 (3), 399–420. doi:10.18268/bsgm2011v63n3a3

Glumac, B., and Spivak-Birndord, M. L. (2002). Stable isotope of carbon as an invaluable stratigraphic tool: an example from the Cambrian of the northern Appalachians, USA. *Geology* 30 (6), 563–566. doi:10.1130/0091-7613(2002)030<0563:SIOCAA>2.0.CO;2

Gómez-pérez, I. (2003). An early Jurassic deep-water stromatolitic bioherm related to possible methane seepage (Los Molles Formation, Neuquen, Argentina). *Palaeogeogr. Palaeoclimatol. Palaeoecol.* 201, 21–49. doi:10.1016/S0031-0182(03)00508-X

Grimes, S. T., Brock, F., Rickard, D., Davies, K. L., Edward, D., Briggs, D. E., et al. (2001). Understanding fossilization: experimental pyritization of plants. *Geology* 29, 123–126. doi:10.1130/0091-7613(2001)029<0123:ufepop>2.0.co;2

Grunsky, E. C. (2010). The interpretation of geochemical survey data: geochemistry. *Explor. Environ. Anal.* 10, 27–74. doi:10.1144/1467-7873/09-210

Hatch, J. R., and Leventhal, J. S. (1992). Relationship between inferred redox potential of the depositional environment and geochemistry of the Upper Pennsylvanian (Missourian) stark shale member of the Dennis limestone, Wabaunsee County, Kansas, U.S.A. *Chem. Geol.* 99, 65–82. doi:10.1016/0009-2541(92)90031-Y

Hu, M. Y. (1994). Geochemical characters and environmental significance of Ordovician carbonate rocks in Kepingarea, Tarim basin. *Oil and Gas Geol.* 15 (2), 158–163. doi:10.11743/ogg19940208

Huang, B. C., Zhou, Y. X., and Zhu, R. X. (2008). Discussions on Phanerozoic evolution and formation of continental China, based on paleomagnetic studies. *Earth Sci. Front.* 15 (3), 348–359. 1005-2321(2008)03-0348-12.

Huang, S. J. (1997). A study on carbon and strontium isotopes of Late Palaeozoic carbonate rocks in the Upper Yangtze platform. *Acta Geol. Sin.* 71 (1), 45–53. doi:10.1093/humrep/17.6.1604

Huerta-Diaz, M. A., and Morse, J. W. (1992). Pyritization of trace metals in anoxic marine sediments. *Geochimica Cosmochimica Acta* 56, 2681–2702. doi:10.1016/0016-7037(92)90353-k

Ishikawa, T., Ueno, Y., Shu, D., Li, Y., Han, J., Guo, J., et al. (2014). The $d^{13}C$ excursions spanning the Cambrian explosion to the Canglangpuian mass extinction in the Three Gorges area, South China. *Gondwana Res.* 25, 1045–1056. doi:10.1016/j.gr.2013.03.010

James, N. P., and Klappa, C. F. (1983). Petrogenesis of Early Cambrian reef limestones, Labrador, Canada. *J. Sediment. Petrol* 53, 1051–1096. doi:10.1306/212F831E-2B24-11D7-8648000102C1865D

James, N. P., and Kobluk, D. R. (1978). Lower Cambrian patch reefs and associated sediments: southern Labrador, Canada. *Sedimentology* 25, 1–35. doi:10.1111/j.1365-3091.1978.tb00299.x

Jiang, Z. X. (2010). *Sedimentology*. Beijing: Petroleum Industry Press.

Katrin, H., Foster, W. J., Sylvain, R., Daniel, B., Julie, R. V., Aymon, B., et al. (2018). The formation of microbial-metazoan bioherms and biostromes following the latest permian mass extinction. *Gondwana Res.* 61, 187–202. doi:10.1016/j.gr.2018.05.007

Kaufman, A. J., Hayes, J. M., Knoll, A. H., and Germs, G. J. B. (1991). Isotopic compositions of carbonates and organic carbon from upper Proterozoic successions in Namibia, stratigraphic variation and the effects of diagenesis and metamorphism. *Precambrian Res.* 49, 301–327. doi:10.1016/0301-9268(91)90039-D

Kaufman, A. J., and Knoll, A. H. (1995). Neoproterozoic variations in the C isotopic composition of seawater stratigraphic and biogeochemical implications. *Precambrian Res.* 73, 27–49. doi:10.1016/0301-9268(94)00070-8

Keith, M. L., and Weber, J. N. (1964). Carbon and oxygen isotopic composition of selected limestones and fossils. *Geochimica Cosmochimica Acta* 28 (10/11), 1787–1816. doi:10.1016/0016-7037(64)90022-5

Kopaska-merkel, D. C., and Haywick, D. W. (2001). Carbonate mounds: Sedimentation, organismal response, and diagenesis. *Sediment. Geol.* 145, 157–159. doi:10.1016/s0037-0738(01)00145-2

Kryc, K. A., Murray, R. W., and Murray, D. W. (2003). Al-to-oxide and Ti-to-organic linkages in biogenic sediment: relationships to paleo-export production and bulk Al/Ti. *Earth Planet. Sci. Lett.* 211, 125–141. doi:10.1016/S0012-821X(03)00136-5

Large, D. J., Sawlowicz, Z., and Spratt, J. A. (1999). A cobaltite-framboidal pyrite association from the Kupferschiefer: possible implications for trace element

behaviour during the earliest stages of diagenesis. *Mineral. Mag.* 63, 353–361. doi:10.1180/002646199548574

Lee, J. H., Chen, J., and Chough, S. K. (2012). Demise of an extensive biostromal microbialite in the Furongian (late Cambrian) Chaomidian Formation, Shandong Province, China. *Geosciences J.* 16, 275–287. doi:10.1007/s12303-012-0027-2

Leggitt, V. L., and Cushman, R. A. (2001). Complex caddisfly-dominated bioherms from the Eocene Green River Formation. *Sediment. Geol.* 145 (3), 377–396. doi:10.1016/S0037-0738(01)00155-5

Li, D., Ling, H., Jiang, S., Pan, J., Chen, Y., Cai, Y., et al. (2009). New carbon isotope stratigraphy of the Ediacaran-Cambrian boundary interval from SW China: Implications for global correlation. *Geol. Mag.* 146 (4), 465–484. doi:10.1017/S0016756809006268

Li, Q. W., Jin, Z. K., and Jiang, F. J. (2014). Carbon and oxygen isotope analysis method for dolomite formation mechanism: A case study from Proterozoic dolomite in Yanshan area. *Lithol. Reserv.* 26 (4), 117–122. 1673-8926(2014)04-0117-06. doi:10.3969/j.issn.1673-8926.2014.04.017

Liu, D., Chen, Z. Q., Adam, D. W., Fang, Y. H., Huang, X. Q., Wu, S. Q., et al. (2024). Revisiting the Yudongzi microbialites (basal Triassic, northwestern Sichuan, South China): Fabric textures and paleoenvironmental implication. *Glob. Planet. Change* 232, 104334. doi:10.1016/j.gloplacha.2023.104344

Luo, B. W., Wei, G. Q., Yang, W., and Dong, C. Y. (2013). Reconstruction of the late Sinian paleo-ocean environment in Sichuan basin and its geological significance Basin. *Geol. China* 40 (4), 1099–1111. doi:10.1007/s10854-013-1233-z

Matthew, S. F., and Max, K. L. (2024). "Demystifying diagenesis: The future of diagenetic inquiry in the geosciences," in *Treatise on geochemistry*. Third edition (Elsevier), 249–314. doi:10.1016/B978-0-323-99762-1.00062-0

McCrea, J. M. (2004). On the Isotopic Chemistry of Carbonates and a Paleotemperature Scale. *J. Chem. Phys.* 18, 849–857. doi:10.1063/1.1747785

McManus, J., Berelson, W. M., Klinkhammer, G. P., Hammond, D. E., and Holm, C. (2005). Authigenic uranium: relationship to oxygen penetration depth and organic carbon rain. *Geochimica Cosmochimica Acta* 69, 95–108. doi:10.1016/j.gca.2004.06.023

Mei, M. X., Ma, Y. S., Mei, S. L., and Hu, J. Z. (1997). Framwork of Cambrian sedimentary sequence and evolution of carbonate platform in North China. *Geoscience* 11 (3), 275–282.

Mei, M. X., Muhammad, R., Khalid, L., Liu, Z. L., Mohamed, S. A., and Douaa, F. (2023). Biohermal complex dominated by microbial carbonates from the early Miaolingian (lower Cambrian) Maozhuang Formation, North China. *Facies* 69, 17. doi:10.1007/s10347-023-00673-8

Meng, H., Ren, Y., Zhong, D. K., Gao, C. L., Gao, Z., Wang, D., et al. (2016). Geochemical characteristic and its palaeoenvironmental implication of Cambrian Longwangmiao Formation in eastern Sichuan Basin, China. *Nat. Gas. Geosci.* 27 (7), 1299–1311. doi:10.11764/j.issn.1672-1926.2016.07.1299

Murphy, M. A., and Sumner, D. Y. (2010). Variations in Neoarchean microbialite morphologies: Clues to controls on microbialite morphologies through time. *Sedimentology* 55, 1189–1202. doi:10.1111/j.1365-3091.2007.00942.x

Myers, K. J., and Wignall, P. B. (1987). Understanding Jurassic organic-rich mudrocks—new concepts using gamma-ray spectrometry and palaeoecology: examples from the Kimmeridge Clay of Dorset and the Jet Rock of Yorkshire. *Mar. Clastic Sedimentol.*, 172–189. doi:10.1007/978-94-009-3241-8_9

Myrow, P. M., Tice, L., Archuleta, B., Clark, B., Taylor, J. F., and Ripperdan, R. L. (2004). Flat-pebble conglomerate: Its multiple origins and relationship to metre-scale depositional cycles. *Sedimentology* 51, 973–996. doi:10.1111/j.1365-3091.2004.00657.x

Octavian, C., and Duncan, B. (2020). Sequence stratigraphy in organic-rich marine mudstone successions using chemostratigraphic datasets. *Earth-Science Rev.* 203, 103–137. doi:10.1016/j.earscirev.2020.103137

Patterson, J. H., Ramsden, A. R., and Dale, L. S. (1986). Geochemistry and mineralogical residences of trace elements in oil shales from Julia Creek, Queensland, Australia. *Chem. Geol.* 55 (1/2), 1–16. doi:10.1016/0009-2541(88)90137-4

Pratt, B. R. (2002). Storms versus tsunamis: Dynamic interplay of sedimentary, diagenetic, and tectonic processes in the Cambrian of Montana. *Geology* 30, 423–426. doi:10.1130/0091-7613(2002)030<0423:svtdio>2.0.co;2

Pratt, B. R., and Bordonar, O. L. (2007). Tsunamis in a stormy sea: Middle Cambrian inner-shelf limestones of western Argentina. *J. Sediment. Res.* 77, 256–262. doi:10.2110/jsr.2007.032

Pruss, S. B., Finnegan, S., Fischer, W. W., and Knoll, A. H. (2010). Carbonates in skeleton-poor seas: New insights from Cambrian and Ordovician strata of Laurentia. *Palaios* 25, 73–84. doi:10.2110/palo.2009.p09-101r

Riding, R. (2006). Microbial carbonate abundance compared with fluctuations in metazoan diversity over geological time. *Sediment. Geol.* 185, 229–238. doi:10.1016/j.sedgeo.2005.12.015

Riding, R., and Liang, L. (2005). Geobiology of microbial carbonates: metazoan and seawater saturation state influences on secular trends during the Phanerozoic. *Palaeogeogr. Palaeoclimatol. Palaeoecol.* 219, 101–115. doi:10.1016/j.palaeo.2004.11.018

Riding, R. E. (1991). *Calcareous algae and stromatolites*. Berlin: Springer, Verlag.

Riding, R. E. (2000). Microbial carbonates: The geological record of Calcified Bacterial-Algal Mats and Biofilms. *Sedimentology* 47 (Suppl. 1), 179–214. doi:10.1046/j.1365-3091.2000.00003.x

Riding, R. E. (2002). Structure and composition of organic reefs and carbonate mud mounds: concepts and categories. *Earth-Science Rev.* 58, 163–231. doi:10.1016/S0012-8252(01)00089-7

Rimmer, S. M. (2004). Geochemical paleoredox indicators in Devonian–Mississippian black shales, Central Appalachian Basin (USA). *Chem. Geol.* 206 (3-4), 373–391. doi:10.1016/j.chemgeo.2003.12.029

Ronald, B., and Carol, D. (2013). *Essentials of igneous and metamorphic petrology*. Cambridge University Press.

Samankassou, E. (2001). Internal structure and depositional environment of Late Carboniferous mounds from the San Emiliano Formation, Cármenes syncline, Cantabrian Mountains, Northern Spain. *Sediment. Geol.* 145, 235–252. doi:10.1016/s0037-0738(01)00150-6

Shao, L. Y., Dou, J. W., and Zhang, P. F. (1996). Palaeogeographic significance of oxygen and carbon isotopes in Late Permian rocks of southwest China. *Geochimica* 25 (6), 575–581. doi:10.19700/j.0379-1726.1996.06.007

Shao, L. Y., and Jones, T. P. (1999). Carbon isotopes and the strati-graphical implication of the Late Permian Carbonates in Central Guangxi. *Acta Sedimentol. Sin.* 17 (1), 84–88. doi:10.3969/j.issn.1000-0550.1999.01.013

Shevelkova, A. N., Sal'nikoV, Y. I., Kuz'mina, N. L., Ryabov, A. D., and Brantley, S. L. (1996). The size distribution of framboidal pyrite in modern sediments: An indicator of redox conditions. *Geochimica Cosmochimica Acta* 60, 3897–3912. doi:10.1016/0016-7037(96)00209-8

State, L. (2015). Partitional clustering algorithms. *Comput. Rev.* 56, 409–410. doi:10.1007/978-3-319-09259-1

Tian, J. C., and Zeng, Y. F. (1995). The evolution pattern of the carbon and oxygen isotopes in the Permian marine carbonate rocks from Guizhou. *J. Chengdu Univ. Technol.* 22 (1), 78–82.

Tribovillard, N., Algeo, T. J., Lyons, T., and Riboulleau, A. (2006). Trace metals as paleoredox and paleoproductivity proxies: An update. *Chem. Geol.* 232, 12–32. doi:10.1016/j.chemgeo.2006.02.012

Wang, J., Zuo, R., and Caers, J. (2017). Discovering geochemical patterns by factor-based cluster analysis. *J. Geochem. Explor.* 181, 106–115. doi:10.1016/j.gexplo.2017.07.006

Wang, P. W., Si, C. S., Zhang, R. H., Li, X. J., Ma, L. Q., Huang, L., et al. (2016). Characteristic of the Cambrian carbonate paleo-ocean environment in the Dianqianbei Depression and its geological significance. *Acta Sedimentol. Sin.* 34 (5), 811–818. doi:10.14027/j.cnki.cjxb.2016.05.001

Wanty, R. B., and Goldhaber, M. B. (1992). Thermodynamics and kinetics of reactions involving vanadium in natural systems: accumulation of vanadium in sedimentary rocks. *Geochimica Cosmochimica Acta* 56, 1471–1483. doi:10.1016/0016-7037(92)90217-7

Wignall, P. B., and Twitchett, R. J. (1996). Oceanic anoxia and the end Permian mass extinction. *Science* 272, 1155–1158. doi:10.1126/science.272.5265.1155

Wilkin, R. T., and Barnes, H. L. (1997). Formation processes of framboidal pyrite. *Geochimica Cosmochimica Acta* 61, 323–339. doi:10.1016/s0016-7037(96)00320-1

Woo, J., and Chough, S. H. (2010). Growth patterns of the Cambrian microbialite: Phototropism and speciation of Epiphyton. *Sediment. Geol.* 229, 1–8. doi:10.1016/j.sedgeo.2010.05.006

Wotte, T., Alvaro, J. J., Shields, G. A., Brown, B., Brasier, M. D., and Veizer, J. (2007). C-O- and Sr-isotope stratigraphy across the Lower-Middle Cambrian Transition of the Cantabrian zone (Spain) and the Montagne Noire (France), West Gondwana. *Palaeogeogr. Palaeoclimatol. Palaeoecol.* 256, 47–70. doi:10.1016/j.palaeo.2007.09.002

Wu, Y. Y., Zhang, T. S., Lü, J. L., and Liu, Y. (2017). The sedimentological characteristics of microbialites of the Cambrian in the vicinity of Beijing, China. *J. Palaeogeogr.* 6 (2), 117–131. doi:10.1016/j.jop.2017.03.003

Xu, Z. J., Lan, Y. Z., Cheng, R. H., and Li, S. L. (2017). Carbonate geochemical record of sea-level change of Lunshan Formation in Lower Ordovician in Jurong area. *J. Jilin Univ. (Earth Sci. Ed.)* 47 (5), 1458–1470. doi:10.13278/j.cnki.jjuese.201705110

Yamashita, Y., Takahashi, Y., Haba, H., Enomoto, S., and Shimizu, H. (2007). Comparison of reductive accumulation of Re and Os in seawater–sediment systems. *Geochimica Cosmochimica Acta* 71, 3458–3475. doi:10.1016/j.gca.2007.05.003

Yang, Z. G. (2004). *Marine Geology*. Jinan: Shandong Education Press.

Yun, H., Zhang, X. L., and Reitner, J. (2024). Microstructure and chancelloriid sclerites within a microbial buildup of the Wirrealpa Limestone (Cambrian Stage 4), South Australia. *Palaeogeogr. Palaeoclimatol. Palaeoecol.* 655, 112526. doi:10.1016/j.palaeo.2024.112526

Zhu, M., Zhang, J., Li, G., and Yang, A. (2004). Evolution of Cisotopes in the Cambrian of China: Implications for Cambrian subdivision and trilobite mass extinctions. *Géobios* 37, 287–301. doi:10.1016/j.geobios.2003.06.001

Zhu, X. M. (2008). *Sedimentary petrology*. Beijing: Petroleum Industry Press.